# A low-cost, sulfurization free approach to control optical and electronic properties of $Cu_2ZnSnS_4$ via precursor variation

Saatviki Gupta[1,2], Thomas J. Whittles[3], Yogita Batra[1], Vibha Satsangi[2], Satheesh Krishnamurthy[4], Vinod R. Dhanak[3] and Bodh Raj Mehta[1*]

[1]*Department of Physics, Indian Institute of Technology Delhi, Hauz Khas, New Delhi – 110016, India*

[2]*Department of Physics & Computer Science, Dayalbagh Educational Institute, Agra-282005, India*

[3]*Department of Physics, University of Liverpool, Liverpool L69 3BX, UK*

[4]*Department of Engineering and Innovation, The Open University, Milton Keynes, MK7 6AA, UK*

[*]**Email address of corresponding author: brmehta@physics.iitd.ernet.in**

**Abstract**

Thin films of $Cu_2ZnSnS_4$ (CZTS) were synthesized via a low cost, wet chemical technique of chemical bath deposition (CBD). In the first part of this study, the chemical composition ratio S/(Cu+Zn+Sn) was varied keeping Cu/(Zn + Sn) and Zn/Sn ratios constant to study the effect of sulfur variation. Detailed electrical and optical characterization has been carried out using UV-Vis spectroscopy, x-ray diffraction, x-ray photoelectron spectroscopy, Raman spectroscopy and Kelvin probe force microscopy (KPFM) techniques. The results of the present study confirm that near ideal stoichiometry could be achieved in CZTS by adding excess thiourea in a controlled manner which eliminated the need for an additional step of sulfurization. Using the stoichiometric sample as the basis, in the second part of the study Cu/(Zn+Sn) and Zn/Sn was varied and it was found that the electronic properties of CZTS in terms of band gap, work function and valence band edge position could be controlled by precursor variation. KPFM was used to qualitatively evaluate the photoresponse of the films and the Cu-poor, Zn-rich samples showed the best photoresponse out of all the samples which has been attributed to a decrease in the $Cu_{Zn}$ type defects. The study thus demonstrates a scalable and low-cost technique to grow CZTS absorber layers for solar cells with control over its electronic properties which is important for effective device operation.

**Keywords:** CZTS, precursor variation, band structure, Kelvin probe force microscopy

## 1. Introduction

Low cost, environmentally friendly and large scale photovoltaic (PV) energy generation requires a semiconductor absorber material that has a high absorption coefficient, large carrier diffusion length, suitable band gap and good junction quality. Additionally, an ideal PV absorber layer should consist of elements that are abundantly available

in nature and can be synthesized at a reasonably low cost. One of the top contenders in the search for an ideal PV absorber is $Cu_2ZnSnS_4$ (CZTS), a quaternary semiconductor compound with a I2-II-IV-VI4 type structure with properties very similar to those of CIGS without being constituted of costly and rare earth elements [1,2].

CZTS as a material provides two unique challenges in terms of ease of synthesis and achieving phase purity. The first problem is of finding the optimal, low-cost route to synthesizing device-grade films and this has led to diverse research on synthesis techniques. CZTS films have been deposited using a number of physical and chemical means. Physical methods include thermal evaporation, sputtering and pulsed laser deposition [3-7]. However, these methods are expensive compared to simpler wet-chemical methods as they require the use of vacuum equipment [8]. Therefore, chemical based methods which include sol-gel synthesis, successive ionic layer adsorption and reaction, chemical bath deposition (CBD), electrodeposition and nanocrystalline ink synthesis are quite promising and have shown good device efficiencies [9-18]. The second challenge lies in the need to synthesize stoichiometric films in a repeatable manner. Being a multi-element material, there are numerous unwanted secondary phases and material defects that form spontaneously during the film's growth [19]. This makes maintaining control over the composition of CZTS, while preserving film quality extremely difficult. Sulfur loss is one of the most common problems in CZTS that leads to the requirement of high-temperature sulfurization to obtain stoichiometric CZTS films [20-22]. Thus the basis of the problem lies in retaining the balance between the four constituting elements, i.e. copper, zinc, tin and sulfur. Overall, the purity of the final film is determined by the reaction rates and kinetics of the synthesis technique being used, and it is also affected by the type, and quantity of precursors chosen. Consequently, there is a need for a detailed and comprehensive study on the effect of stoichiometry and precursor ratios on the structure and semiconducting properties of CZTS films.

Reported studies in which the Cu concentration was varied have shown its effect on band gap, resistivity and grain size [23-26]. Similarly studies on Zn and Sn variation also report changes in the band gap of CZTS [20, 27-31]. Sulfur content variation has been demonstrated by changing the sulfurization time of the CZTS film and it has been shown that as sulfurization time (and therefore sulfur content) increases, band gap decreases and this has been ascribed to an improvement in the film's quality [32]. The changes observed in band gap are usually attributed to changes in the bonding between atoms or formation of high/low band gap secondary phases [24,30,33]. Changes in the population of defects (and defect clusters) caused by elemental variation have also been shown to affect carrier density and unit cell volume [25,27,34].

In the past few years, Kelvin probe force microscopy (KPFM) has emerged as an ideal tool to measure the surface potential (and using it, the work function) of materials at the nano and micro scale. In CZTS, KPFM has most commonly been used to correlate grain boundary potentials with film quality and has been used to demonstrate that there exists a higher, positive surface potential at the grain boundaries which is beneficial [35-37]. KPFM scans have been used to map the presence of secondary phases such as $Cu_xS$ and ZnS on the surface of CZTS films

[38,39] and then to see the changes in work function after their removal by etching agents such as KCN, HCl etc. [39-41]. Spatial variations in surface potential across the surface of CZTSSe films have also been studied by KPFM as a function of S/(S+Se) ratio [42].

Similarly, it was also observed that x-ray photoelectron spectroscopy (XPS) has not been widely applied as a tool to help map the band structure of CZTS. XPS core-level data is frequently used to analyze purity and composition of CZTS films [43-47] and the effect of S/(S+Se) ratio on the electronic structure of $CZTS_xSe_{(1-x)}$ has been studied by XPS and inverse photoelectron spectroscopy (IPES) [48].

In most of the studies mentioned above, one (or sometimes two) of the elemental ratios have been varied to change the film composition and the effects on band gap and phase purity investigated. For a complete understanding of synthesis conditions on CZTS, it is important to carry out a comprehensive study to investigate the effect of Cu, Zn, Sn and S precursor ratios on the important semiconducting parameters (band gap, work function and valence band edge position) in a single study. This will provide a clear overview of how the semiconducting properties of CZTS are altered with different elemental compositions.

In the present study, a low-cost wet-chemical technique to obtain stoichiometric CZTS films has been optimized by adding excess thiourea in a controlled manner. This eliminated the need for additional sulfurization. The effect of precursor variation (by varying S, Cu and Zn quantities) was examined on the structural, optical and electronic properties of the material using x-ray diffraction, Raman spectroscopy, UV-Visible spectroscopy, XPS and KPFM. Kelvin probe force microscopy has been demonstrated as a simple tool to quantitatively assess the CZTS films as an absorber material by measuring the improvement in photoresponse as Cu and Zn quantities change. Finally, a correlation has been established between change in precursor ratios and its effect on the band structure.

The major findings of the present study show that addition of excess thiourea as a sulfur precursor yields CZTS films with near-ideal stoichiometry. Using these films as a starting point, as Cu content is decreased and Zn content increased, the films exhibit a distinct increase in band gap, lowering of work function and the distance between the Fermi level and valence band maximum increases. KPFM maps of the sample surface show an appreciable improvement in the photoresponse with the difference between dark and light surface potential increasing from ~3 mV (Cu-rich, Zn-poor films) to ~54 mV (extremely Cu-poor, Zn-rich films). This improvement has been explained on the basis of a decrease in $Cu_{Zn}$ defect states which are known to cause deep acceptor levels in the band gap.

## 2. Experimental details

Synthesis of CZTS films was carried out using chemical bath deposition on glass and indium-tin-oxide (ITO) coated glass substrates. Prior to deposition, the substrates were cleaned by sonicating in a mild laboratory detergent in de-ionized water followed by propanol and finally acetone to remove inorganic and organic impurities. The

precursors used for synthesis were copper acetate ($Cu(CH_3COO)_2$), zinc acetate ($Zn(CH_3CO2)_2$), stannous chloride ($SnCl_2$) and thiourea ($CH_4N_2S$) with methanol ($CH_3OH$; HPLC grade) as the solvent. All of there were purchased from Merck chemicals and were at-least, or greater that 99% purity. Seven samples (S1 to S3 with sulfur variation and S4 to S7 with Cu and Zn variation) were prepared in 50 ml of methanol each. The molarities of each of the precursors for the samples were chosen according to the following table

| Sample Name | Elemental ratios |
|---|---|
| **S1** | Cu/(Zn+Sn) = 1; Zn/Sn = 1; S = 4 |
| **S2** | Cu/(Zn+Sn) = 1; Zn/Sn = 1; S = 8 |
| **S3** | Cu/(Zn+Sn) = 1; Zn/Sn = 1; S = 20 |
| **S4 (Cu rich, Zn poor)** | Cu/(Zn+Sn) = 2 ; Zn/Sn = 0.9 ; S = 20 |
| **S5 (Cu poor, Zn rich)** | Cu/(Zn+Sn) = 0.9 ; Zn/Sn = 1.1 ; S = 20 |
| **S6 (Cu poor, Zn rich)** | Cu/(Zn+Sn) = 0.8 ; Zn/Sn = 1.2 ; S = 20 |
| **S7 (Cu poor, Zn rich)** | Cu/(Zn+Sn) = 0.7 ; Zn/Sn = 1.3 ; S = 20 |

**Table 1.** Precursor ratios for samples S1 to S7

Separate beakers were used for carrying out the reactions simultaneously. After the precursors had been weighed and added to their respective beakers, 50 ml of methanol was added to each and the solutions were allowed to stir until all the salts had dissolved completely. Following this, the substrates were dipped into the solution by submerging them completely for 30 seconds and then taken out and placed on a clean petri dish. After the first round of dipping, the samples were heated at $250^0$C in an oven for 25 minutes. A thin black film was formed on the substrates indicating the formation of the first layer of CZTS. However the film was non-uniform, therefore, the cycle of dipping and heating was repeated two more times until a uniform, black film of CZTS was formed. Finally a separate annealing was carried out at $350^0$C (in air on a hot plate) to ensure a well-formed, homogenous film. After this the samples were stored in vacuum until further analysis.

The films were characterized by x-ray diffraction (using a Phillips X'Pert Pro MPD diffractometer), Raman spectroscopy (Renishaw inVia confocal micro-Raman spectrometer; Renishaw Inc., UK) and UV-visible spectroscopy (Perkin Elmer Lambda - 35). XPS analysis was carried out in a standard ultra-high vacuum (UHV) chamber operating at a base pressure of less than $2\times10^{-10}$ mbar with hydrogen as the main residual gas. The core-level electronic structure and occupied density of states in the valence band were probed by XPS using a SPECS monochromatic Al Kα X-ray source (hν = 1486.6 eV) operating at 200 W, together with a PSP Vacuum Technology electron-energy analyzer operating with a constant pass energy of 10 eV. Calibration of the

spectrometer was performed using a polycrystalline silver foil, cleaned in-vacuo. The Ag 3d5/2 photoelectron line had a binding energy (BE) of 368.3 eV and a full-width at half-maximum (FWHM) of 0.6 eV. The Fermi edge of the silver sample had a spectral width of 0.3 eV. From this calibration, tolerances were determined to be ±0.1 eV for core-level binding energies and ±0.05 eV for the valence band maxima (VBM). High-resolution spectra of the Cu 2p, Zn 2p, Sn 3d and S 2p regions were recorded and fitted using Voigt functions after a Shirley background had been subtracted.

All KPFM measurements were carried out in the non-contact mode on a Veeco Instruments multimode AFM (Nanoscope IIIa with an extender electronics module). A Pt-Ir coated Si cantilever with a radius of curvature of 30 nm and a resonance frequency of ~60 kHz (nominal k = 3 $Nm^{-1}$) was used. The scans were carried out in the lift mode with a typical lift height of 20 nm. Initially scans were carried out for different lift heights from 15 to 50 nm to ensure there was no "cross talk" due to van der Waal's forces. Finally 20 nm was chosen as the lift height for the scans. A white light fibre-optic source with 150 mW $cm^{-2}$ intensity was used for illuminating the sample during the KPFM scans. The source had been previously calibrated using a standard, commercially available silicon solar cell. The KPFM scans of the samples were processed and analyzed using the WsXM software [49] to calculate the value of the average surface potential. The work function has been calculated from the average surface potential using the formula: $\Phi_{SAMPLE} = \Phi_{TIP} + V_{CPD}$. Where $\Phi_{SAMPLE}$ is the work function of the sample (to be calculated), $\Phi_{TIP}$ is the work function of the tip (~4.9 – 5 eV as calibrated using standard HOPG and gold films) and $V_{CPD}$ is the contact potential difference of the sample or the average surface potential over entire scan area. In the case of the instrument we have used, the $V_{CPD}$ is added to the tip's work function because the nullifying voltage during the scan is applied to the sample instead of the tip as has been previously reported in the literature [50,51]. A detailed description of the experimental set up is given elsewhere [52].

## 3. Results and discussion

### 3.1 Sulfur variation (samples S1-S3):

To obtain the ratio of the elements present in the films grown with varying precursor content, EDX analysis was carried out and the data for the three ratios (Cu/(Zn+Sn), Zn/Sn and S/(Cu+Zn+Sn)) is shown below in Table 2.

| Sample Name | Cu/(Zn+Sn) | Zn/Sn | S/(Cu+Zn+Sn) |
|---|---|---|---|
| **S1** | 0.8 | 1.4 | 0.7 |
| **S2** | 1.0 | 1.2 | 0.8 |
| **S3** | 1.2 | 1.1 | 1.1 |

**Table 2**. Elemental ratios as calculated from EDX data for samples S1-S3

As the molarity of the sulfur precursor was increased, the ratio S/(Cu+Zn+Sn) increased from ~0.7 to 1.1 (from S1 to S3). The ideal value for all three ratios is 1 and thus sample S3 is the closest to the correct stoichiometry even without the additional sulfurization step. X-ray diffraction was carried out to confirm the formation of the actual $Cu_2ZnSnS_4$ phase and the resulting patterns are shown in figure 1. The spectra show the characteristic peaks for kesterite CZTS (JCPDS card no. 260575) with 2θ values of 28.5°, 37.73°, 47.3° and 56.16°. However samples S1 and S2 have many secondary phases also present with XRD peaks corresponding to $SnS_x$ and $Cu_xS$ marked in the diffractogram. Specific phases have not been assigned to the peaks as there are many overlaps with very slight differences in 2-theta values. However they definitely belong to tin and copper based secondary phases. As the sulfur content is increased, the formation of the secondary phases decreases and sample S3 shows peaks corresponding only to kesterite $Cu_2ZnSnS_4$ with clear peaks for the (112), (220) and (312) planes and no discernable peaks for other secondary phases. However, it is well known that due to the overlap of the diffraction pattern of the ZnS secondary phase with CZTS, XRD alone cannot confirm the formation of single phase kesterite. Therefore, Raman spectroscopy was carried out on the samples and the results are shown in figure 2. The spectra has been de-convoluted to gain a better understanding of the different phases present in the material and changes in their relative intensity with changes in the precursor ratio. The peaks at ~334 $cm^{-1}$ and ~287 $cm^{-1}$ are the primary and secondary characteristic peaks for kesterite CZTS phase respectively [53-55]. The peaks at ~358 $cm^{-1}$ and ~657 $cm^{-1}$ can be attributed to ZnS [54,56] while the peak at ~471 $cm^{-1}$ belongs to $Cu_{2-x}S$ [54], both of which are unwanted secondary phases. As the quantity of the sulfur precursor is increased, the intensity of the peaks indicating kesterite CZTS phase increase while those for the secondary phases of ZnS and $Cu_{2-x}S$ decrease. Thus, both Raman analysis and x-ray diffraction data clearly confirm the formation of kesterite $Cu_2ZnSnS_4$ phase in sample S3.

The observation of a decrease in unwanted secondary phases with an increase in sulfur precursor may be explained as follows: as the content of the sulfur precursor (thiourea) increases, there is a proportionate increase in the free sulfur available in the reaction solution. This in turn increases the number of metal-sulfur complexes associated with free sulfur which directly leads to an increase in the available CZTS nucleation cites. Such a correlation has previously been observed in CZTS nanocrystals grown using thiourea as the sulfur source [57].

UV-Vis spectroscopy measurements on S1 and S2 showed the onset of absorption to be at ~2.2 eV and 2 eV respectively. This overall higher band edge position may be attributed to the significant presence of high band gap secondary phases such as ZnS, $SnS_x$ and $Cu_xS$ (as also indicated by XRD and Raman analysis). However for sample S3 the onset of absorption is at ~1.58 eV which corresponds well with the range of values reported in the literature for kesterite CZTS [22,58]. This decrease in band gap with increasing sulfur content has been previously reported in CZTS films where it was considered to be indicative of the removal of secondary phases. However it is important to note that in these earlier studies it was done with increasing sulfurization time [59] whereas in the

present case it has been achieved by increasing the sulfur precursor concentration in the starting chemical bath solution and there is no further sulfurization. In addition, as the EDX data shows, the films become slightly Cu-rich as correct stoichiometry is achieved which is a phenomenon that has been observed earlier [60]. When this happens, it leads to a change in the degree of p-d hybridization between the S p-levels and the Cu d-levels. Since the VBM of CZTS is due to anti-bonding of S 3p and Cu 3d orbitals, therefore changes in the band gap may be ascribed to changes in the p-d hybridization. The increase in the hole population reduces the VBM and in turn causes a decrease in the band gap [24]. Thus it is inferred that samples S1 and S2 are not fully formed kesterite CZTS rather they are a mixture of secondary phases, however sample S3 can be called kesterite CZTS ($Cu_2ZnSnS_4$) with almost negligible quantities of these unwanted phases.

To confirm the valence states of the elements present in the CZTS structure, high-resolution XPS was performed on the samples**.** The measurements were carried out after argon ion sputtering for five minutes to remove contaminants present in the top layers of the sample. Survey scans before and after sputtering showed that oxygen and carbon contamination is greatly reduced after this etching treatment. Binding energy values were calculated using the C 1s peak at 284.8 eV as the reference. The XPS spectra of S1, S2 and S3 are shown in figure 3. Part (a) shows the 2p1/2 and 2p3/2 doublet peaks for Cu. Two strong peaks appear at ~932.5 and 952.6 eV with a constant difference of ~19.8 eV which match the standard values for 2p1/2 and 2p 3/2 for the $Cu^+$ state. It's also seen that there is no shoulder peak at 933.7 eV which would have shown the presence of CuO with a $Cu^{2+}$ valency. Moreover, shake-up satellite peaks that appear around 940 to 945 eV for CuO are also not observed. Figure 3 (b) shows the spectra for Zn in S1, S2 and S3. Two clear peaks at ~1022.1 and 1044.6 with a constant separation of ~22.5 eV match well with the standard values for Zn 2p3/2 and 2p1/2 [43-47]. These peaks show the presence of $Zn^{2+}$ in the material. In part (c) of the figure, the peaks at ~485.8 and 494.3 eV with a constant separation of ~8.4 eV match well with the Sn 3d5/2 and 3d3/2 states which indicate the presence of $Sn^{4+}$ [43-47]. In addition to these, all the three samples show the Zn LMM Auger peaks at ~496.5 eV binding energy on the high energy side of the 3d spectrum for Sn.

The S peaks for the three samples have been analyzed in detail by deconvoluting it to gain a better understanding of the species of sulfur present. Figure 3 parts (d), (e) and (f) show the XPS data for sulfur for samples S1, S2 and S3 respectively. It is seen that in all the three cases, two distinct species of sulfur are present which have been marked in the plots. Species 1 has a lower set of binding energies (with S 2p3/2 peaks in the range of ~161.3 eV and S 2p1/2 peaks at ~162.5 eV) as compared to species 2 (with S 2p3/2 peaks in the range of ~162.5 eV and S 2p1/2 peaks at ~163.7 eV). As the quantity of sulfur is increased, the relative intensity of species 2 increases with respect to species 1 within each sample. This can be explained on the basis of the fact that each of these two species indicates sulfur bonding in a unique manner. Species 1 is due to sulfur bonded into the CZTS lattice and matches well with previously reported binding energy values and verifies the presence of the $S^{2-}$ valence state [43-47]. Species 2 has been ascribed to the unreacted thiourea present in the material and the relatively higher values of

binding energies for the S 2p 3/2 peaks at ~162.3 eV (for the =S in $C(NH)_2S$) match with the values reported for thiourea [61,62]. In addition it was observed that in all three samples, even after argon ion sputtering, the signal for nitrogen (attributed to thiourea) persists and its intensity increases from S1 to S3. All these observations correspond well with the fact that the intensity of species 2 is the highest in S3 because this sample had the maximum amount of excess thiourea added to it.

In addition to studying the crystal structure, band gap and valence states, the variation in the position of the Fermi level and its distance from the VBM was also examined. The work functions of the three samples were determined from Kelvin probe force microscopy (KPFM) and the surface scans are shown in figure 4. It was observed that as the quantity of sulfur increases in the samples, the work function correspondingly becomes larger or it can be said that the material becomes more p-type in nature. To further verify this, valence band measurements were carried out, the results of which also showed that the distance between the Fermi level and the VBM decreases from 0.51 eV in S1 to 0.19 eV in S3. This can be explained by the fact that it is known [63,64] that $Cu_{Zn}$ antisites are the most easily formed defect states in CZTS and are the cause for its naturally p-type nature. As correct stoichiometry is achieved, it is seen that the film (sample S3) becomes slightly Cu-rich (from EDX). This leads to the formation of $Cu_{Zn}$ antisites which contribute to the generation of holes in the material [24]. This increase in the hole population is reflected in the Fermi level moving down (increase in work function) and the distance between it and the VBM decreasing. In addition, as the sulfur precursor content increases in the films, the availability of free sulfur increases and in turn, the formation of unwanted secondary phases decreases (as seen from the XRD and Raman data). Many of these secondary phases are actually n-type materials and can compensate the number of holes available for conduction in the inherently p-type CZTS. Thus a decrease in the number of competing phases can also effectively increases the concentration of holes and cause a shifting of the Fermi level towards the VBM.

The schematic diagram in figure 5 depicts the changes observed in the band structure of the material as the sulfur precursor is increased from sample S1 to S3. It can be seen that as sulfur incorporation increases, the band gap decreases, work function increases and the distance between the Fermi level and VBM decreases. Thus sample S3 has near-ideal stoichiometry for CZTS.

**3.2 Cu and Zn variation (samples S4-S7)**:

Studies have shown that a Cu-poor and Zn-rich phase is desired in CZTS so that formation of $Cu_{Zn}$ antisites is inhibited (as they form deep acceptor levels detrimental to device performance) along with phases such as like $Cu_2SnS_3$ which are formed with Zn-poor conditions. However, with compositions that are Zn-rich, a competitive phase such as ZnS can be easily formed and this must be minimized. Therefore it is necessary to find the optimal Cu to Zn ratios for the best device performance and this is the aim of the second part of this study. The present

study is different from those reported previously in the fact that KPFM has been used as a tool to qualitatively and quantitatively evaluate the improvement in photoresponse of the films with changing Cu and Zn ratios.

In the previous section detailed characterization showed that sample S3 has a stoichiometry consistent with kesterite $Cu_2ZnSnS_4$ when the starting precursor ratios were taken as: Cu/(Zn+Sn) = 1, Zn/Sn = 1 and S = 20. Considering this sample as stoichiometrically correct $Cu_2ZnSnS_4$, the current section details the variation in Cu and Zn ratios while keeping Sn and S constant (same as the content used in S3). Specifically, the two ratios (Cu/Zn + Sn) and (Zn/Sn) were varied with the aim of mapping the resulting change in the material's band structure. Four samples denoted by S4, S5, S6 and S7 were prepared and their starting precursor ratios are given in Table 1. Since it is well known that a Cu-poor, Zn-rich composition is the best from the point of view of application to devices for CZTS [25,33], it was decided to keep one sample Cu-rich and the other three Cu-poor and Zn-rich to facilitate comparison in their properties. X-ray diffraction was carried out first to study the phase purity of the samples. Figure 6, parts (a), (b), (c) and (d) show the x-ray diffractograms for S4, S5, S6 and S7 respectively. For sample S4, in addition to the standard peaks for kesterite CZTS at 28.4°, 47.6° and 56.0° there are a number of secondary peaks in the scan. These can be attributed to numerous $SnS_x$ and $Cu_xS$ phases which have been clearly marked in the figure. Amongst these, the phases arising due to copper are the most prominent and this is expected since S4 is extremely Cu-rich. In S5 (the first Cu-poor and Zn-rich sample), there is a drastic fall in the intensity of the secondary phases and a few low intensity peaks are still visible for $Cu_xS$ and $SnS_x$. In S6 and S7 (which are even more Cu-poor and Zn-rich), all the secondary, 'spurious' phases disappear completely leaving only the three peaks belonging to kesterite CZTS.

Results of Raman spectroscopy are shown in figure 7. All the samples show that the characteristic peak for the A1 mode for CZTS at ~333 $cm^{-1}$ as well as a small peak at ~474 $cm^{-1}$ which indicates the presence of $Cu_xS$. However it can be seen that as the samples transition from Cu-rich to Cu-poor, the $Cu_xS$ peak becomes very small and in addition, the shoulder peak at ~287 $cm^{-1}$ can be seen to be becoming stronger which also corresponds to kesterite CZTS. Therefore the data from Raman spectroscopy corroborates the conclusions we had drawn from the XRD scans.

Band gap measurements were carried out by UV-Visible spectroscopy and the data (in the form of Tauc's plots) is shown in figure 8. For sample S4 it can be seen that the band gap is at ~ 1.36eV. As the samples move towards an increasingly Cu-poor and Zn-rich composition, a clear increase in the band gaps is visible with sample S7 showing a value of ~1.62 eV. Thus, there is a trend of increasing band gap energy as the samples become progressively Cu-poor. The phenomenon of band-gap shrinkage with an increasing Cu/Sn ratio (or band gap increase with a decreasing Cu/Sn ratio) has been previously studied [27] and a number of theories proposed such as (i) bandgap variation because of stannite-kesterite polymorphic transformations; (ii) the existence of solid solutions between CZTS and its secondary phases such as SnS or $SnS_2$ and (iii) shrinkage due to a large concentration of acceptor

defects which reduces the bandgap by the formation of an 'acceptor band' near the valence band of the material. In the present case the sample S4 may have a similar acceptor band near its valence band edge due to the fact that it is Cu-rich and Zn-poor which can give rise to a high population of $Cu_{Zn}$ type defect states that act as acceptors leading to an overall smaller bandgap. As the Cu content decreases in S5, S6 and S7 the band gap correspondingly increases.

Valence states of the different elements in the samples were determined by XPS analysis. Data analysis was carried out as detailed previously in the experimental section. The peaks in figure 9 (a) at 932.1 eV and 951.8 eV with a separation of 19.7 eV correspond well with Cu 2p 3/2 and 2p 1/2 and are indicative of the formation of $Cu^{+1}$. Similarly in figure 9 (b), the peaks at 1021.3 eV and 1044.5 eV correspond to the Zn 2p 3/2 and 2p 1/2 doublet and show a separation of 23.2 eV confirming Zn to be in its $Zn^{2+}$ state. Figure 9 part (c) shows that Sn is present in its $Sn^{4+}$ state with peaks at ~484.8 eV and 493.1 eV with a separation of 8.3 eV in the form of the Sn 3d 5/2 and 3d 3/2 peaks. Finally, the peaks marked as S' in figure 9 parts (d), (e), (f) and (g) confirm the presence of the sulphide $S^{2-}$ valence state with 2p 3/2 and 2p 1/2 peaks at ~161.6 eV and 162.7 eV with a peak separation of 1.1 eV. As in the case of samples S1 to S3, a second set of peaks (denoted by S") have also been fit which have been attributed to the unreacted sulfur in the form of thiourea. In addition, it can be clearly seen that as the samples become Cu-poor and Zn-rich, the intensity of the Cu 2p doublet peaks decreases and those of the Zn 2p doublet increases. There is a small difference in the peak positions in case of Sn (~1.3 eV) between S4 and S7 however, the binding energies corresponding to these values still lie within the standard interval reported for $Sn^{4+}$. Thus all the valence states of the samples are consistent with those expected of the kesterite CZTS phase [43-47].

In addition to the analysis of the binding energy values, the change in the two sulfur ratios (sulfur that has bonded within the CZTS structure and unreacted thiourea) in terms of the areas of the fitted peaks was calculated and the data is shown in table 3. Here, S' is the area of the peaks corresponding to reacted sulfur which was 'species 1' in the last section and S" corresponds to unreacted sulfur which was 'species 2' previously. The data shows that the ratio S'/S" increases from S4 to S7. From this it is inferred that the Cu-poor and Zn-rich growth condition promotes the incorporation of sulfur into the crystal structure of the film.

| **Sample Name** | **S' (reacted)** | | **S" (unreacted)** | | **Ratios** | |
|---|---|---|---|---|---|---|
| | **Area 1** | **Area 2** | **Area 1** | **Area 2** | **(S'1 +S'2) /(S"1 + S"2)** | **S'/S"** |
| **S4** | 305.0 | 152.5 | 155 | 77.5 | 457.5/232.5 | 1.96 |
| **S5** | 584.9 | 292.4 | 253.5 | 126.7 | 877.3/380.2 | 2.30 |
| **S6** | 356.4 | 178.2 | 148.8 | 74.4 | 534.6/223.2 | 2.39 |
| **S7** | 337.2 | 168.6 | 122.2 | 61.1 | 505.8/183.3 | 2.75 |

**Table 3.** Ratios of reacted to unreacted sulfur for samples S4 to S7

Surface potential measurements and corresponding work function calculations for the films were done using KPFM and the results are shown in figure 10 (a). The data clearly shows that as the films go from being Cu-rich, Zn-poor to Cu-poor, Zn-rich, the work function values fall consistently. Samples S4 - S7 show a work function of 5.47, 5.42, 5.36 and 5.15 eV, respectively. It can be seen that unlike samples S1 to S3, a change in the Cu and Zn content causes large changes in the work function with a difference of almost 320 mV between S4 and S7. From this trend it can be inferred that as Cu decreases and Zn increases in the samples, the Fermi level of the semiconductor shifts up thereby indicating a decreased p-type behaviour from samples S4 to S7. Valence band offset measurements were performed on these samples and the results are shown in figure 10 parts (b - e). On moving from sample S4 to S7, the distance between the valence band edge and the Fermi level increases from 0.14 eV for S4 to 0.49 eV for S7. Thus the results of the KPFM measurement and valence band offset measurements both prove the same point that removal of copper and introduction of excess zinc causes the Fermi level to move upward (work function to decrease) and the VBM to move away from it. This is probably due to the decreasing Cu content causing a fall in the number of $Cu_{Zn}$ defects which leads to a fall in the number of holes in the films.

Surface potential (SP) measurements in the dark and under illumination were also carried out and the average SP distribution is obtained from these images and plotted in the form of histograms. The difference between dark and light surface potentials is a measure of the photoresponse of a particular sample. Figure 11 (a), (b), (c) and (d) show the SP histograms in the dark and light for samples S4 to S7 respectively while parts (e), (f), (g) and (h) show the 3D AFM topography images of the same samples. For sample S4, there is a negligible shift in SP as it goes from dark to light and this shift is of the order of ~3 mV. For sample S5, the photoresponse only improves very slightly (~8 mV). However in the case of S6 and S7 there is an appreciable shift in SP of ~34 mV and 54 mV respectively under illumination. The final band diagrams of the samples with Cu and Zn variation are shown in figure 12 along with the trends observed in their optical and electrical properties.

It has been previously shown through extensive theoretical simulations as well as many experimental studies that it is the presence of $Cu_{Zn}$ type antisite defects and $V_{Cu}$ (copper vacancies) which primarily give rise to the inherent p-type nature of CZTS [63,64]. These defects have been shown to not change the overall electronic structure of CZTS but place the Fermi energy at the valence band maxima thus leading to the formation of a large number of shallow hole states [65]. However, between these two defect types, $Cu_{Zn}$ has a lower energy of formation (0.01eV) as compared to $V_{Cu}$ (0.57eV) therefore it is predicted that $Cu_{Zn}$ is the dominant acceptor defect in CZTS grown under equilibrium conditions [64]. It has also been shown that the (0/-) i.e. acceptor transition energy for $Cu_{Zn}$ is 0.10 eV above the VBM while for $V_{Cu}$ the same value is 0.02eV. This makes the $Cu_{Zn}$ level a deep defect state which can be detrimental to the performance of the material as an absorber layer in a photovoltaic device by lowering the open circuit voltage. It is to suppress the formation of these deep level defects that Cu-poor, Zn-rich conditions are preferred in the synthesis of CZTS.

In the present study, the aim was to be able to decrease the number of $Cu_{Zn}$ type antisite defects so as to improve the photoresponse of the material. These deep level defects would have acted as traps for photogenerated carriers thereby leading to a poor photoresponse (as seen in S4 which is extremely Cu-rich). The results of the various characterizations carried out show that there is indeed a decrease in the work function accompanied by a significant improvement in the photoresponse of the film as the material is made Cu-poor and Zn-rich which we can attribute to a fall in the number of $Cu_{Zn}$ type defects.

## 4. Conclusions

The present study demonstrates that changing the precursor composition in the chemical bath allows: (i) the growth of stoichiometric CZTS by the use of excess thiourea in a controlled manner and (ii) the ability to manipulate the band structure of CZTS in terms of band gap, work function and valence band edge position by controlling Cu/(Zn+Sn) and Zn/Sn ratios.

On varying the sulfur content, the XPS results clearly show that sulfur is present in the form of two different species, the first of unreacted sulfur (corresponding to thiourea) and secondly sulfur from the CZTS phase. Increase in sulfur content results in arresting the growth of secondary phases and phase pure CZTS films are grown without the need of additional sulfurization. It is also shown that Cu-poor and Zn-rich growth conditions result in CZTS films with a negligible quantity of secondary phases and lead to increasing band gaps and decreasing work functions which have been attributed to a fall in the deep level $Cu_{Zn}$ type defects which would otherwise have trapped photogenerated carriers and degraded the device performance. These results are further confirmed by an enhancement in the photoresponse of the film which is shown by a larger difference between dark and light surface potential values in Cu-poor, Zn-rich films. Though further research and optimization is needed to improve the quality of these films and to demonstrate their use in device fabrication, however the present study is an important step towards the development of low-cost absorber materials which do not require sulfurization. If applied to large scale device fabrication, the growth technique described in this study is not only faster and uncomplicated but also makes the process economically viable. The control demonstrated in this study over the optical and electronic properties by varying the initial precursor composition is extremely useful in the fabrication of solar cell devices. This ability to tune the band structure also opens up many new avenues in other applications such as in photocatalysis, sensing and water splitting all of which require the material to have certain, very specific properties. The technique demonstrated here allows control over these properties thus facilitating the diverse use of this non-toxic, earth abundant material.

## 5. Acknowledgements

BRM acknowledges the support provided by a Schlumberger Chair Professorship and the financial support provided by the Ministry of Information Technology; SG would like to thank the Council of Scientific and Industrial Research (CSIR), India, for providing financial assistance in the form of a Senior Research Fellowship; TJW acknowledges funding through the UK Engineering and Physical Sciences Research Council (EPSRC) (Grant No. EP/J500471/1) and VRD acknowledges support through the Capital for Great Technologies – Grid Scale Energy Storage Programme. The authors are thankful to FIST (DST Govt. of India) UFO scheme of IIT Delhi for providing Raman facility.

## References

[1] S. Siebentritt and S. Schorr, Kesterites - a challenging material for solar cells, Prog. Photov. 20 (2012), 512–519

[2] X. Liu, Y. Feng, H. Cui, F. Liu, X. Hao, G. Conibeer, D.B. Mitzi, M. Green, The current status and future prospects of kesterite solar cells: a brief review, Prog. Photovolt: Res. Appl. (2016)

[3] J.S. Seol, S.Y. Lee, J.C. Lee, H.D. Nam, K.H. Kim, Electrical and optical properties of $Cu_2ZnSnS_4$ thin films prepared by rf magnetron sputtering process, Sol. Energ. Mat. Sol. Cells 75 (2003), 155-162.

[4] A.I. Inamdar, S. Lee, K.Y. Jeon, C.H. Lee, S.M. Pawar, R.S. Kalubarme, C.J. Park, H. Im, W. Jung, H. Kim, Optimized fabrication of sputter deposited $Cu_2ZnSnS_4$ (CZTS) thin films, Solar Energy 91 (2013), 196-203

[5] C. Shi, G. Shi, Z. Chen, P. Yang, M. Yao, Deposition of $Cu_2ZnSnS_4$ thin films by vacuum thermal evaporation from single quaternary compound source, Mater Lett 73 (2012), 89-91

[6] L. Sun, J. He, H. Kong, F. Yue, P. Yang, J. Chu, Structure, composition and optical properties of $Cu_2ZnSnS_4$ thin films deposited by Pulsed Laser Deposition method, Sol. Energ. Mat. Sol. Cells 95 (2011), 2907-2913

[7] L. Sun, J. He, Y. Chen, F. Yue, P. Yang, J. Chu, Comparative study on $Cu_2ZnSnS_4$ thin films deposited by sputtering and pulsed laser deposition from a single quaternary sulfide target, J. Cryst. Growth 361 (2012) 147-151

[8] S. Abermann, Non-vacuum processed next generation thin film photovoltaics: towards marketable efficiency and production of CZTS based solar cells, Solar Energy 94 (2013) 37-70

[9] K. Tanaka, N. Moritake, H. Uchiki, Preparation of $Cu_2ZnSnS_4$ thin films by sulfurizing sol-gel deposited precursors, Sol. Energ. Mat. Sol. Cells 91(2007) 1199-1201

[10] Z. Su, K. Sun, Z. Han, H. Cui, F. Liu, Y. Lai, J. Li, X. Hao, Y. Liu, M.A. Green, Fabrication of $Cu_2ZnSnS_4$ solar cells with 5.1% efficiency via thermal decomposition and reaction using a non-toxic sol-gel route, J. Mater. Chem. A 2, no. 2 (2014) 500-509.

[11] Y. Sun, , K. Zong, H. Zheng, H. Wang, J. Liu, H. Yan, M. Zhu, Ethylene glycol-based dip coating route for the synthesis of $Cu_2ZnSnS_4$ thin film, Mater Lett 92 (2013) 195-197

[12] K. Patel, V. Kheraj, D.V. Shah, C. J. Panchal, N.G. Dhere, $Cu_2ZnSnS_4$ thin-films grown by dip-coating: Effects of annealing, J. Alloys Compd. 663 (2016) 842-847

[13] J.J. Scragg, P.J. Dale, L.M. Peter, Synthesis and characterization of $Cu_2ZnSnS_4$ absorber layers by an electrodeposition-annealing route, Thin Solid Films 517(2009) 2481-2484.

[14] C.P Chan, H. Lam, C. Surya, Preparation of $Cu_2ZnSnS_4$ films by electrodeposition using ionic liquids, Sol. Energ. Mat. Sol. Cells 94(2010) 207-211

[15] S. Kahraman, S. Çetinkaya, H. A. Çetinkara, H. S. Güder, A comparative study of $Cu_2ZnSnS_4$ thin films growth by successive ionic layer adsorption–reaction and sol-gel methods, Thin Solid Films 550(2014) 36-39

[16] S.S. Mali, P.S. Shinde, C.A. Betty, P.N. Bhosale, Y.W. Oh, P.S. Patil, Synthesis and characterization of $Cu_2ZnSnS_4$ thin films by SILAR method, J. Phys. Chem. Solids 73(2012) 735-740

[17] Q. Guo, H.W. Hillhouse, R. Agrawal, Synthesis of $Cu_2ZnSnS_4$ nanocrystal ink and its use for solar cells, JACS 131(2009) 11672-11673

[18] C. Steinhagen, M.G. Panthani, V. Akhavan, B. Goodfellow, B. Koo, B.A. Korgel, Synthesis of $Cu_2ZnSnS_4$ nanocrystals for use in low-cost photovoltaics, JACS 131(2009) 12554-12555

[19] M. Kumar, A. Dubey, N. Adhikari, S. Venkatesan, and Q. Qiao, Strategic review of secondary phases, defects and defect-complexes in kesterite CZTS–Se solar cells, Energy Environ Sci 8(2015) 3134-3159

[20] C. Platzer-Björkman, J. Scragg, H. Flammersberger, T. Kubart, M. Edoff, Influence of precursor sulfur content on film formation and compositional changes in $Cu_2ZnSnS_4$ films and solar cells, Sol. Energ. Mat. Sol. Cells 98 (2012) 110-117

[21] A. Emrani, P. Vasekar, C. R. Westgate, Effects of sulfurization temperature on CZTS thin film solar cell performances, Solar Energy 98 (2013) 335-340

[22] J. He, L. Sun, K. Zhang, W. Wang, J. Jiang, Y. Chen, P. Yang, J. Chu, Effect of post-sulfurization on the composition, structure and optical properties of $Cu_2ZnSnS_4$ thin films deposited by sputtering from a single quaternary target, Appl. Surf. Sci. 264(2013) 133-138

[23] V.G. Rajeshmon, M.R.R Menon, C. S. Kartha, and K. P. Vijayakumar, Effect of copper concentration and spray rate on the properties $Cu_2ZnSnS_4$ thin films deposited using spray pyrolysis J Anal Appl Pyrol 110(2014) 448-454

[24] A.V. Moholkar, S.S. Shinde, G. L. Agawane, S. H. Jo, K.Y. Rajpure, P. S. Patil, C. H. Bhosale, and J. H. Kim, Studies of compositional dependent CZTS thin film solar cells by pulsed laser deposition technique: An attempt to improve the efficiency, J Alloy Compd 544 (2012) 145-151

[25] J. Márquez, M. Neuschitzer, M. Dimitrievska, R. Gunder, S. Haass, M. Werner, Y. E. Romanyuk, S. Schorr, N. M. Pearsall, and I. Forbes, Systematic compositional changes and their influence on lattice and optoelectronic properties of $Cu_2ZnSnS_4$ kesterite solar cells, Sol. Energ. Mat. Sol. Cells 144 (2016) 579-585

[26] O. Vigil-Galán, M. Espíndola-Rodríguez, Maykel Courel, X. Fontané, D. Sylla, V. Izquierdo-Roca, A. Fairbrother, E. Saucedo, and A. Pérez-Rodríguez, Secondary phases dependence on composition ratio in sprayed $Cu_2ZnSnS_4$ thin films and its impact on the high power conversion efficiency, Sol. Energ. Mat. Sol. Cells 117 (2013) 246-250

[27] C. Malerba, F. Biccari, C.L.A. Ricardo, M. Valentini, R. Chierchia, M. Müller, A. Santoni, E. Esposito, P. Mangiapane, P. Scardi, A. Mittiga, CZTS stoichiometry effects on the band gap energy, J. Alloys Compd. 582(2014) 528-534

[28] M. Patel, I. Mukhopadhyay and A. Ray, Structural, optical and electrical properties of spray-deposited CZTS thin films under a non-equilibrium growth condition, J. Phys. D: Appl. Phys. 45(2012) 445103

[29] V. G Rajeshmon, C.S. Kartha, K.P. Vijayakumar, C. Sanjeeviraja, T. Abe, and Y. Kashiwaba, Role of precursor solution in controlling the opto-electronic properties of spray pyrolysed $Cu_2ZnSnS_4$ thin films, Solar Energy 85(2011) 249-255

[30] J. Park, , M. Song, W. M. Jung, W. Y. Lee, H. Kim, Y. Kim, C. Hwang, and I.W. Shim, Syntheses of $Cu_2SnS_3$ and $Cu_2ZnSnS_4$ nanoparticles with tunable Zn/Sn ratios under multibubble sonoluminescence conditions, Dalton Transactions 42(2013) 10545-10550

[31] J. Chen, Q. Chen, Y. Ni, Y. Yamaguchi, T. Wang, Z. Jia, X. Dou and S. Zhuang, The synthesis of $Cu_2ZnSnS_4$ nanoparticles via an open-air solution route: influences of Zn precursor content, J Sol-Gel Sci Techn 75(2015) 25-30

[32] J. H. N. Tchognia, Y. Arba, B. Hartiti, A. Ridah, J.M. Ndjaka and P. Thevenin, Effect of sulfurization time on properties of $Cu_2ZnSnS_4$ thin films obtained by sol–gel deposited precursors, Opt Quant Electron 48(2016) 1-7

[33] K. Woo, Y. Kim, and J. Moon, A non-toxic, solution-processed, earth abundant absorbing layer for thin-film solar cells, Energy Environ Sci 5(2012) 5340-5345

[34] C.H. Ruan, C.C. Huang, Y.J. Lin, G.R. He, H.C. Chang, Y.H. Chen, Electrical properties of $Cu_xZn_ySnS_4$ films with different Cu/Zn ratios, Thin Solid Films 550(2014) 525-529

[35] G.Y. Kim, A.R. Jeong, J.R. Kim, W. Jo, D.H. Son, D.H. Kim and J.K. Kang, Surface potential on grain boundaries and intragrains of highly efficient $Cu_2ZnSn(S,Se)_4$ thin-films grown by two-step sputtering process, Sol. Energ. Mat. Sol. Cells 127(2014) 129-135

[36] J. B Li, V. Chawla and B.M. Clemens, Investigating the role of grain boundaries in CZTS and CZTSSe thin film solar cells with scanning probe microscopy, Adv. Mater 24(2012) 720-723

[37] G. Y. Kim, J. R. Kim, W. Jo, D. H. Son, D.H. Kim and J.K. Kang, Nanoscale observation of surface potential and carrier transport in $Cu_2ZnSn(S,Se)_4$ thin films grown by sputtering-based two-step process, Nanoscale Res. Lett. 9(2014) 1-5

[38] G.Y. Kim, D.H. Son, T. T. T. Nguyen, S. Yoon, M. Kwon, C.W. Jeon, D.H. Kim, J.K. Kang, and W. Jo, Enhancement of photo-conversion efficiency in $Cu_2ZnSn(S,Se)_4$ thin-film solar cells by control of ZnS precursor-layer thickness, Prog Photovoltaics Res Appl 24(2016) 292-306

[39] G.Y. Kim, W. Jo, K.D. Lee, H.S. Choi, J.Y. Kim, H.Y. Shin, T.T.T. Nguyena, S. Yoona, B.S. Joo, M. Gu, M. Han, Optical and surface probe investigation of secondary phases in $Cu_2ZnSnS_4$ films grown by electrochemical deposition, Sol. Energy Mater. Sol. Cells 139(2015) 10-18

[40] G.Y. Kim, J. R. Kim, W. Jo, K. D. Lee, J. Y. Kim, T. T. T. Nguyen and S. Yoon, Effects of $Cu_{2-x}S$ phase removal on surface potential of $Cu_2ZnSnS_4$ thin-films grown by electroplating, Curr. Appl. Phys. 14(2014) 1665-1668

[41] M. E. Erkan, V. Chawla, I. Repins and M. A. Scarpulla, Interplay between surface preparation and device performance in CZTSSe solar cells: Effects of KCN and $NH_4OH$ etching, Sol. Energy Mater. Sol. Cells 136(2015) 78-85

[42] M, Salvador, S. M. Vorpahl, H. Xin, W. Williamson, G. Shao, D. U. Karatay, H. W. Hillhouse, and D. S. Ginger, Nanoscale surface potential variation correlates with local S/Se ratio in solution-processed CZTSSe solar cells, Nano Lett. 14(2014) 6926-6930

[43] M. Cao and Y. Shen, A mild solvothermal route to kesterite quaternary $Cu_2ZnSnS_4$ nanoparticles, J. Cryst. Growth 318(2011) 1117-1120

[44] S. W. Shin, S. M. Pawar, C. Y. Park, J. H. Yun, J.H. Moon, J. H. Kim and J. Y. Lee, Studies on $Cu_2ZnSnS_4$ (CZTS) absorber layer using different stacking orders in precursor thin films, Sol. Energy Mater. Sol. Cells 95(2011) 3202-3206

[45] S. W. Shin, J. H. Han, C. Y. Park, S.R. Kim, Y. C. Park, G. L. Agawane, A.V. Moholkar, J.H. Yund, C. H. Jeonge, J. Y. Leea and J. H. Kim, A facile and low cost synthesis of earth abundant element $Cu_2ZnSnS_4$ (CZTS) nanocrystals: Effect of Cu concentrations, J. Alloys Compd. 541 (2012) 192-197

[46] G. Gordillo, C. Calderon and P. B. Perez, XPS analysis and structural and morphological characterization of $Cu_2ZnSnS_4$ thin films grown by sequential evaporation, Appl. Surf. Sci 305(2014) 506-514.

[47] J. Wang, P. Zhang, X. Song and L. Gao, Surfactant-free hydrothermal synthesis of $Cu_2ZnSnS_4$ (CZTS) nanocrystals with photocatalytic properties, RSC Advances 53(2014) 27805-27810

[48] N. Terada, S. Yoshimoto, K. Chochi, T. Fukuyama, M. Mitsunaga, H. Tampo, H. Shibata, K. Matsubarab, S. Nikib, N. Sakaic, T. Katouc, H. Sugimoto, Characterization of electronic structure of $Cu_2ZnSn(S_xSe_{1-x})_4$ absorber layer and $CdS/Cu_2ZnSn(S_xSe_{1-x})_4$ interfaces by in-situ photoemission and inverse photoemission spectroscopies, Thin Solid Films 582(2015) 166-170

[49] I. Horcas, Rs Fernández, J. M. G. Rodriguez, J. Colchero, J. G. Herrero, and A. M. Baro, WSXM: a software for scanning probe microscopy and a tool for nanotechnology, Rev. Sci. Instrum 78 (2007) 013705

[50] W. Melitz, J. Shen, A. C. Kummel and S. Lee, Kelvin probe force microscopy and its application, Surf. Sci. Rep 66(2011) 1-27

[51] V. Kaushik, D. Varandani and B. R. Mehta, Nanoscale Mapping of Layer-Dependent Surface Potential and Junction Properties of CVD-Grown $MoS_2$ Domains, J. Phys. Chem. C 119(2015) 20136-20142.

[52] S. Gupta, Y. Batra, B. R. Mehta and V. R. Satsangi, Study of charge separation and interface formation in a single nanorod CdS-$Cu_xS$ heterojunction solar cell using Kelvin probe force microscopy, Nanotechnology 24(2013) 255703

[53] S.S Mali, B.M. Patil, C.A. Betty, P.N. Bhosale, Y.W. Oh, S.R. Jadkar, R.S. Devan, Y.R. Ma, P.S. Patil, Novel synthesis of kesterite $Cu_2ZnSnS_4$ nanoflakes by successive ionic layer adsorption and reaction technique: characterization and application, Electrochim. Acta 66 (2012) 216-221

[54] A. Shavel, M. Ibáñez, Z. Luo, J.D. Roo, À. Carreté, M. Dimitrievska, A. Genç, M. Meyns, A.P.Rodríguez, M.V. Kovalenko, J. Arbiol, A. Cabot, Scalable heating-up synthesis of monodisperse $Cu_2ZnSnS_4$ nanocrystals Chem. Mater. 28 (2016) 720–726

[55] F. Zhou, F. Zeng, X. Liu, F. Liu, N. Song, C. Yan, A. Pu, J. Park, K. Sun, X. Hao, Improvement of Jsc in a $Cu_2ZnSnS_4$ Solar Cell by Using a Thin Carbon Intermediate Layer at the $Cu_2ZnSnS_4$ /Mo Interface, ACS Appl. Mater. Interfaces 7(2015) 22868-22873

[56] P. A. Fernandes, P.M.P. Salomé, A.F. Da Cunha, Growth and Raman scattering characterization of $Cu_2ZnSnS_4$ thin films, Thin solid films 517(2009) 2519-2523

[57] M.J. Turnbull, S. Khoshmashrab, Z. Wang, R. Harbottle, T.K. Sham, Z. Ding, Controlling $Cu_2ZnSnS_4$ photocatalytic ability through alterations in sulfur availability, Catal. Today 260 (2016) 119-125

[58] B. Shin, O. Gunawan, Y. Zhu, N. A. Bojarczuk, S. J. Chey and S. Guha, Thin film solar cell with 8.4% power conversion efficiency using an earth-abundant $Cu_2ZnSnS_4$ absorber, Prog Photovoltaics Res Appl 21(2013) 72-76

[59] H. Guan, H. Shen, C. Gao, X. He, Sulfurization time effects on the growth of $Cu_2ZnSnS_4$ thin films by solution method, J. Mater. Sci. Mater. Electron. 24(2013) 2667-2671

[60] W.H. Zhou, Y.L. Zhou, J. Feng, J.W. Zhang, S.X. Wu, X.C. Guo and X. Cao, Solvothermal synthesis of flower-like $Cu_2ZnSnS_4$ nanostructures and their application as anode materials for lithium-ion batteries, Chem. Phys. Lett 546 (2012) 115-119

[61] V. Srinivasan and R.A. Walton, X-ray photoelectron spectra of inorganic molecules: Observations concerning the sulfur 2p binding energies in metal complexes of thiourea, Inorg. Chim. Acta 25(1977) L85-L86

[62] T.H. Lee and J.W. Rabalais, X-ray photoelectron spectra and electronic structure of some diamine compounds, J. Electron. Spectrosc. Relat. Phenom. 11(1977) 123-127

[63] S. Chen, X.G. Gong, A. Walsh, S.H. Wei, Defect physics of the kesterite thin-film solar cell absorber $Cu_2ZnSnS_4$, Appl. Phys. Lett. 96(2010) 021902

[64] S. Chen, A. Walsh, X.G. Gong, S.H. Wei, Classification of Lattice Defects in the Kesterite Cu2ZnSnS4 and Cu2ZnSnSe4 Earth-Abundant Solar Cell Absorbers, Adv. Mater. 25(2013) 1522-1539

[65] A. Nagoya, R. Asahi, R. Wahl, G. Kresse, "Defect formation and phase stability of Cu2ZnSnS4 photovoltaic material, Phys. Rev. B 81(2010) 113202.

# Figures

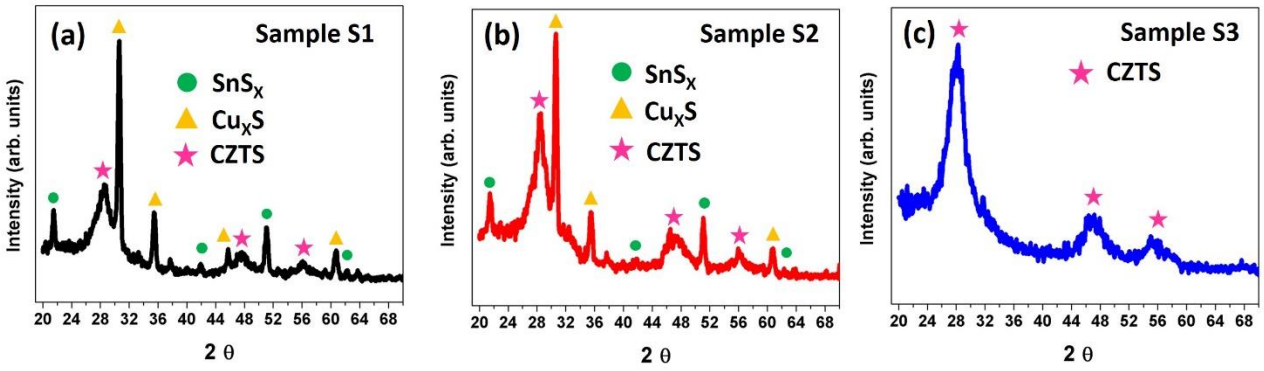


**Figure 1.** X-ray diffraction data for samples (a) S1, (b) S2 and (c) S3.

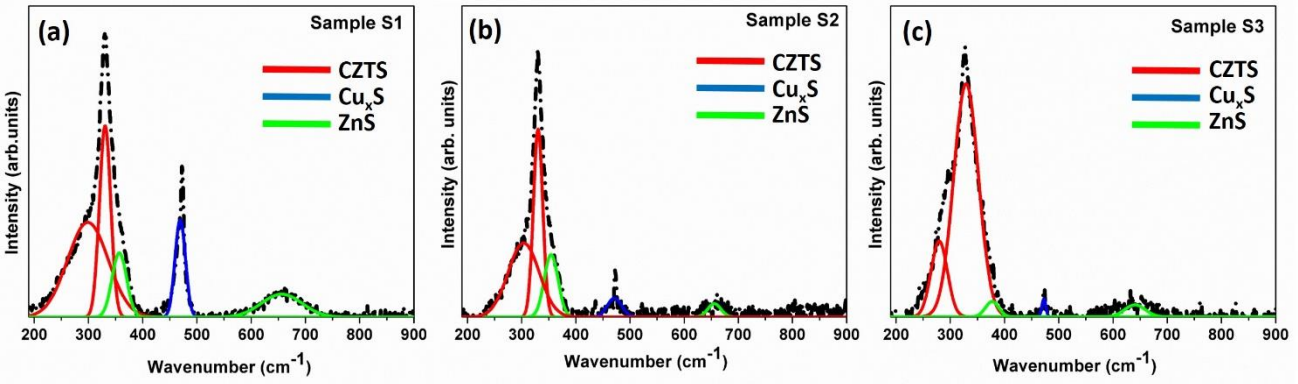


**Figure 2.** Raman spectra for samples S1, S2 and S3. Deconvolution has been carried out to analyze the presence of different phases.

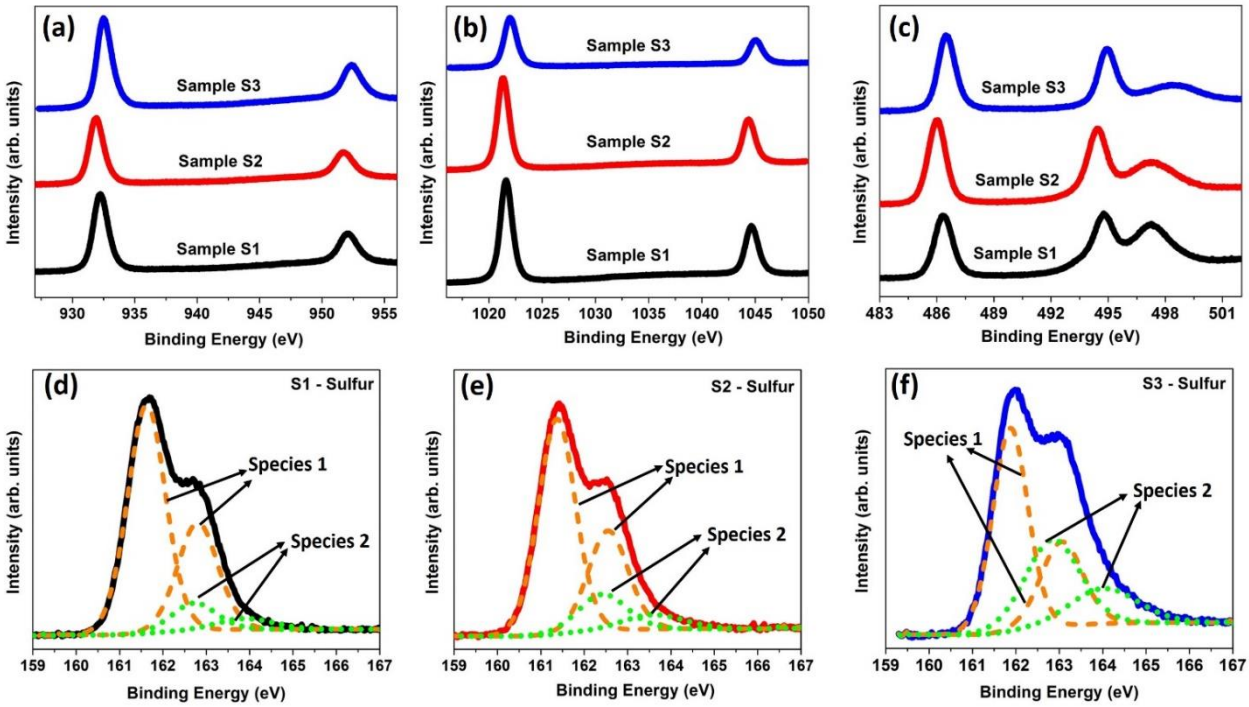


**Figure 3.** XPS spectra for the S1, S2 & S3 samples with (a) Cu 2p3/2 and 2p1/2; (b) Zn 2p3/2 and 2p1/2 and (c) Sn 3d5/2 and 2d3/2 with the Zn L2M45M45 auger peak at ~496.5 eV. Parts (d), (e) and (f) show the S 2p3/2 and 2p1/2 spectra for the two different species of sulfur present in samples S1, S2 and S3 respectively.

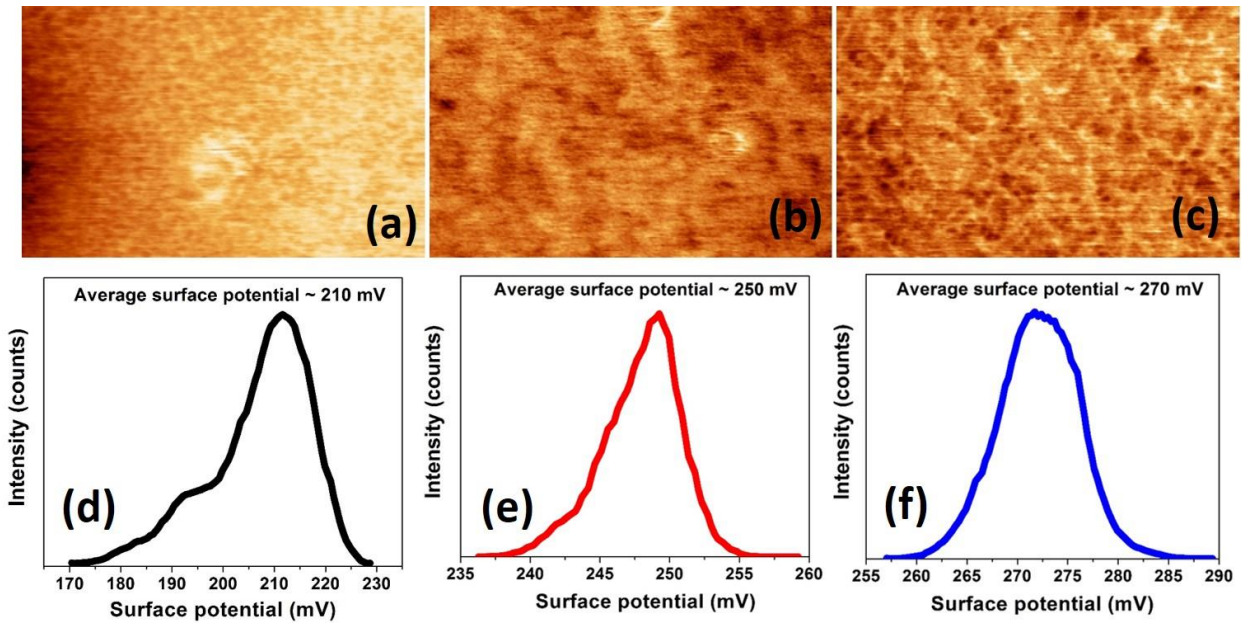


**Figure 4**. Surface potential scans and histograms showing average surface potential for samples: S1 (a) and (d); S2 (b) and (e); S3 (c) and (f) respectively

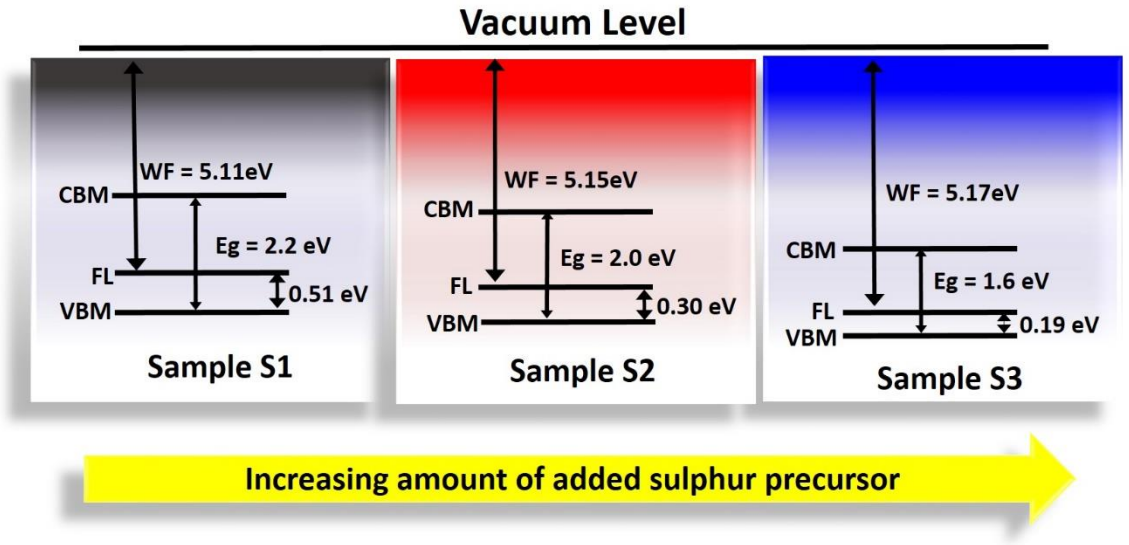


**Figure 5.** Band structure of CZTS samples S1, S2 and S3 derived from the results of the first part of the study. It can be seen that as thiourea content increases, band gap decreases, work function increases and valence band maxima decreases.

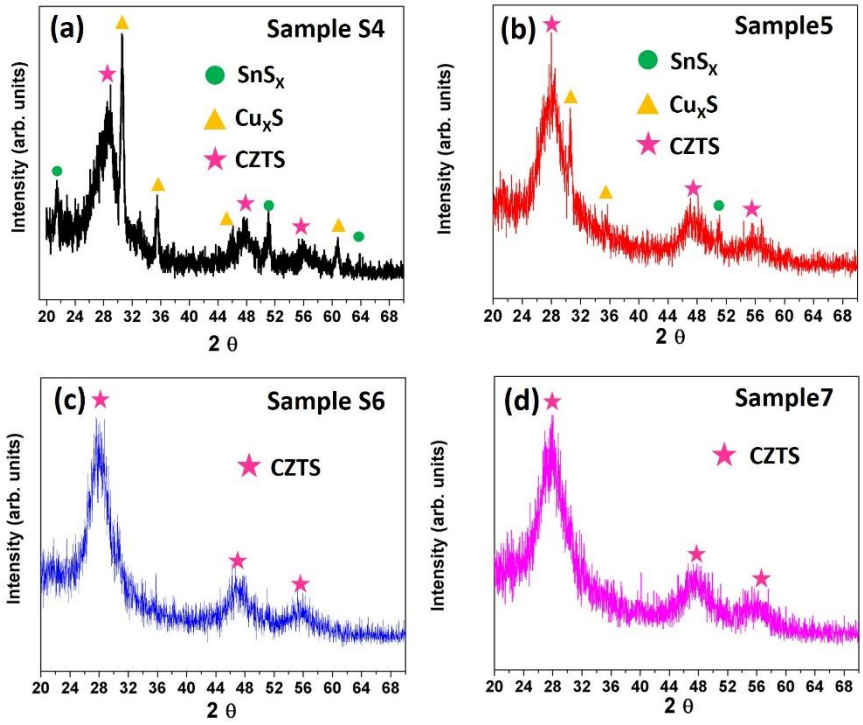


**Figure 6.** X-ray diffraction data for samples (a) S4, (b) S5, (c) S6 and (d) S7

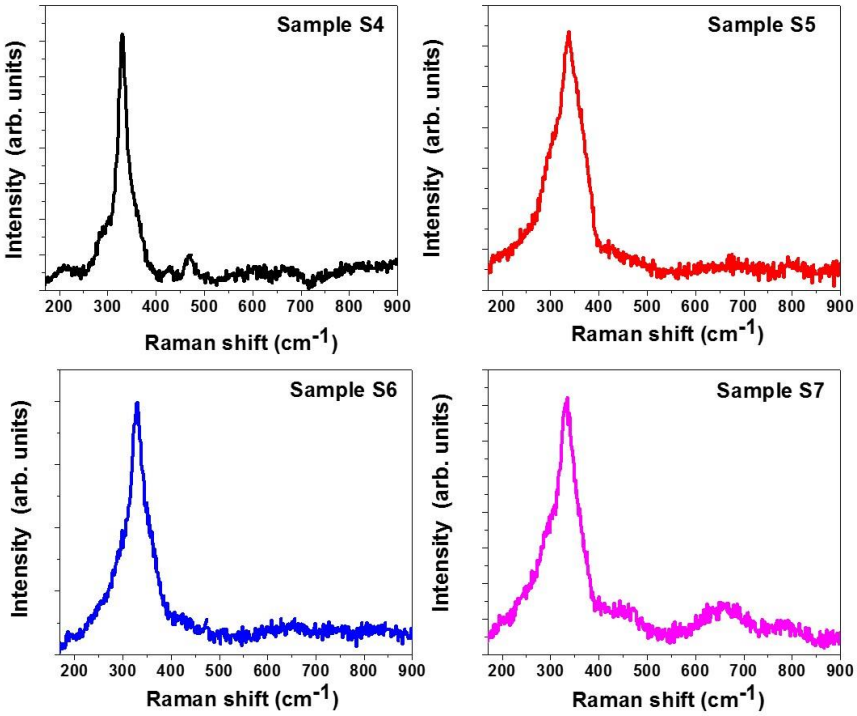


**Figure 7.** Raman spectra for samples S4 to S7. The characteristic CZTS peak at ~333 $cm^{-1}$ is observed in all the samples

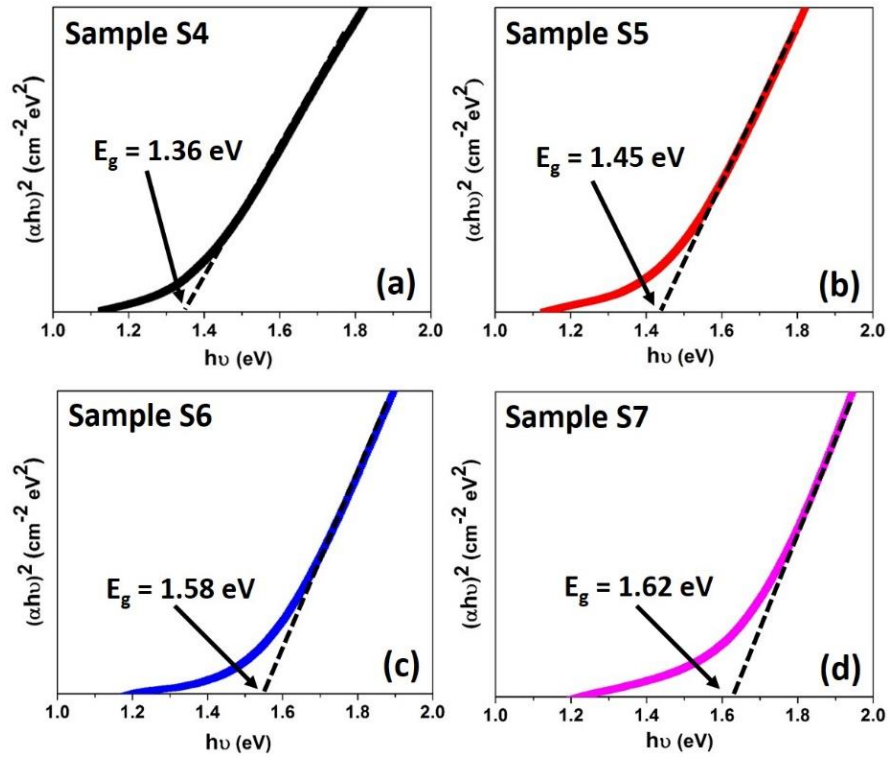


**Figure 8**. Tauc's plot showing a progressive increase in band gap from S4 to S7

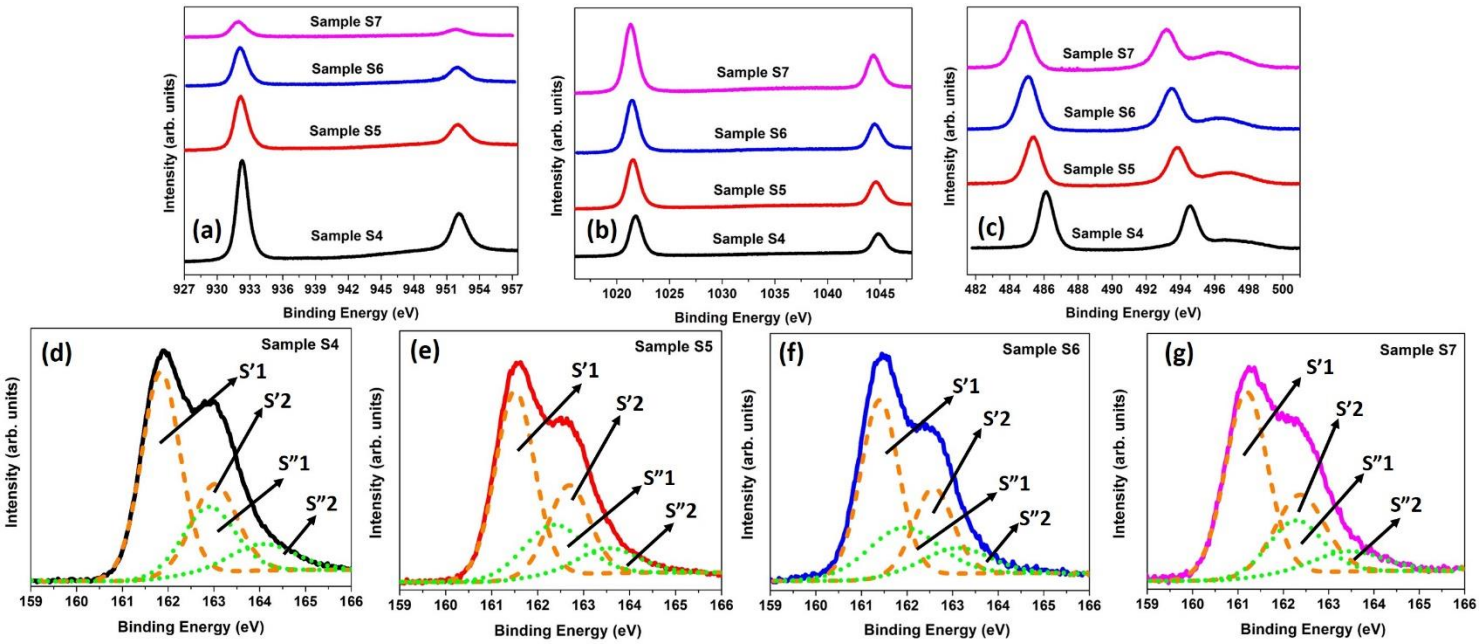


**Figure 9**. XPS analysis of S4 to S7 showing peaks for: (a) Cu 2p 3/2 and 2p ½; (b) Zn 2p 3/2 and 2p ½; (c) Sn 3d 5/2 and 3d 3/2 (and an Auger peak) and (d), (e), (f), (g) for S 2p 3/2 and 2p ½. The fitted peaks corresponding to reacted (S') and unreacted (S") sulfur have been labelled.

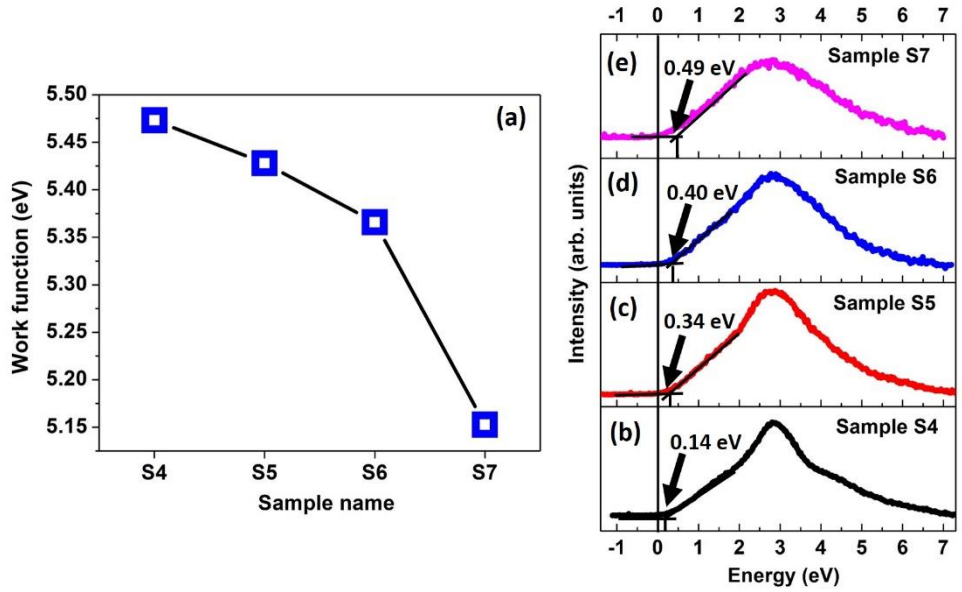


**Figure 10.** (a) Work function variation for S4 to S7; parts (b), (c), (d) and (e) show valence band offset measurements for S4 to S7

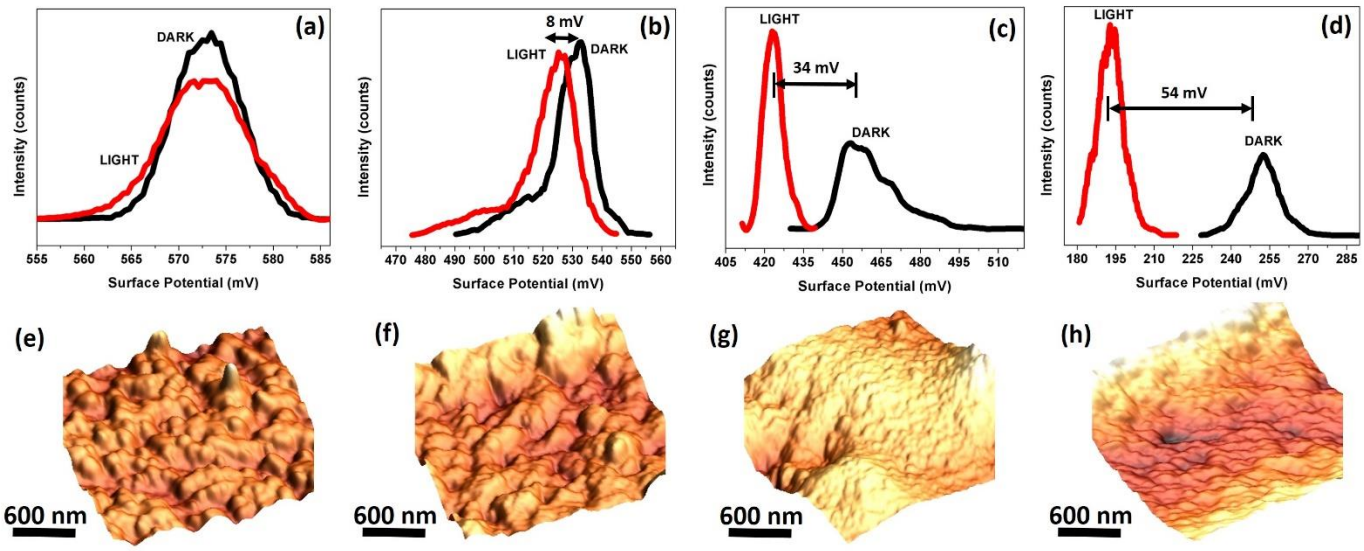


**Figure 11.** Parts **(**a) to (d): show shifts in average surface potential when samples are taken from dark to light; parts (e) to (h) show 3D topography scans of the samples

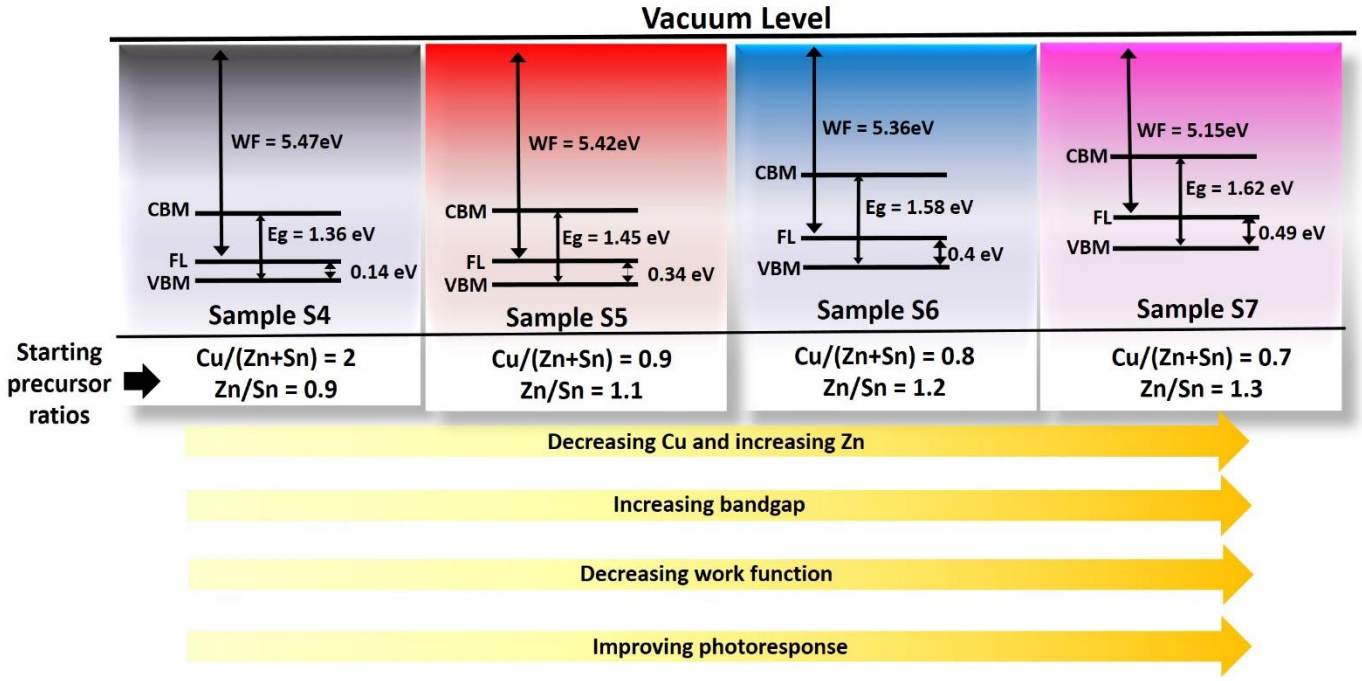


**Figure 12**. Band structure mapping of samples S4, S5, S6 and S7 based on the results of this study (CBM = conduction band minimum, VBM = valence band maximum, FL = Fermi level, WF = work function, Eg = bandgap energy)